Supporting Information

Ultra-high dispersion of Ni-based OER catalysts on graphene 3D networks enhances the in-situ Fe3+ catalytic activation

María González-Ingelmo,[a] Miriam López García, [a] Freddy E. Oropeza, [b] Patricia Álvarez, [a]

Clara Blanco, [a] Ricardo Santamaría [a] and Victoria G. Rocha *[a]

[a] Instituto de Ciencia y Tecnología del Carbono, INCAR-CSIC, Francisco Pintado Fe 26, 33011-Oviedo (Spain)

[b] Photoactivated Processes Unit, IMDEA Energy, Avenida Ramón de la Sagra 3, 28935-Móstoles, Madrid (Spain)

*Corresponding author: Victoria G. Rocha (vgarciarocha@incar.csic.es)

1. Preparation of Fe-free KOH electrolyte

KOH electrolyte was purified for rigorously Fe-free measurements following a procedure reported by Trotochaud et al. [1] In a 30 mL polypropylene centrifuge tube, 0.8 g of $Ni(NO_3)\cdot 6\,H_2O$ were dissolved in 1.6 mL of Milli-Q H2O. 8 mL 1 M KOH were added to form a high-purity $Ni(OH)_2$ precipitate. The mixture was shaken and centrifuged at 4000 rpm for 20 min and the supernatant was decanted. $Ni(OH)_2$ precipitate was washed up to three times by adding 1.6 mL of 1 M KOH and 8 mL of Milli-Q H_2O followed by shaking, centrifugation and decanting. Once $Ni(OH)_2$ was obtained it is used to adsorb Fe impurities present in KOH. Therefore, 20 mL of 1M KOH were added to the solid precipitate and mechanically agitated for at least 10 minutes. The solution was allowed to rest for 3 h. It was then centrifuged at 6000 rpm for 30 minutes. The purified KOH supernatant was collected by filtration through a hydrophilic 0.1μm polyethersulfone filter [2] into a polypropylene bottle for storage and used as Fe-Free KOH.

a

Frequency (%) vs Flake size (μm)

Bars: 0-20 ≈ 12, 20-40 ≈ 57, 40-60 ≈ 23, 60-80 ≈ 6, 80-100 ≈ 1.5

30 μm (scale bar in inset)

b

Intensity (a.u) vs Binding energy (eV)

········ Experimental — Fit
—— C=C & C-C (40.4%) —— C-O (42.4%)
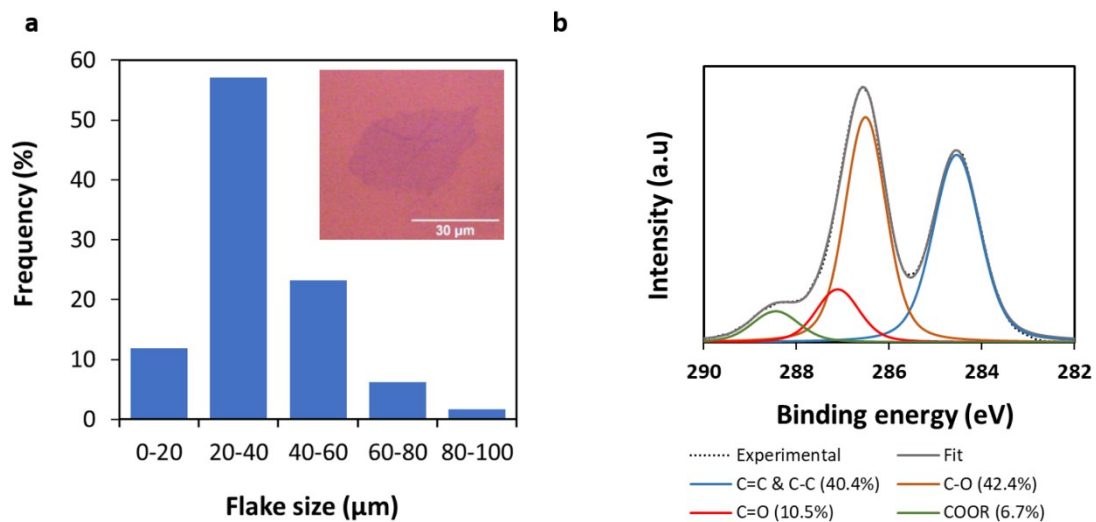—— C=O (10.5%) —— COOR (6.7%)

Figure *S1*|GO characterization. Image **a** shows the distribution of flake size and a flake image taken by optical microscopy (inset) while **b** represents the deconvoluted C1s spectra of GO
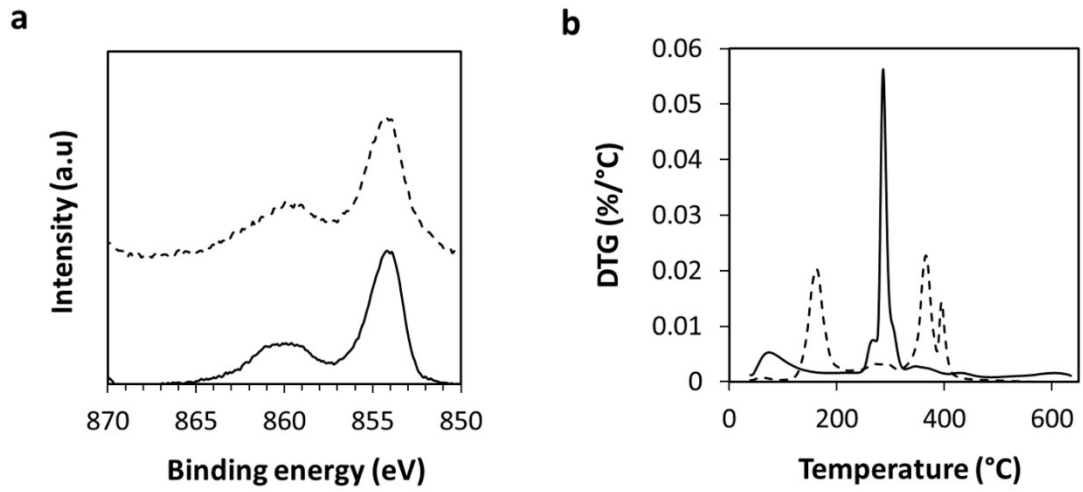
Figure *S2*|NiOHx precursors characterization. a) XPS Ni2p spectra and **b)** weight mass loss curve in air atmosphere up to 650 °C (10°C/min) of the different NiOHx precursors: lactate (solid line) and nitrates (dashed line).

Table *S1*| Formulation and Ni concentration of the hybrid's networks determined by ICP-MS of the hybrid materials.

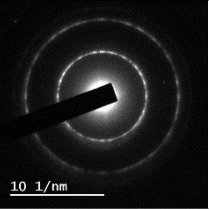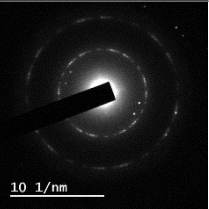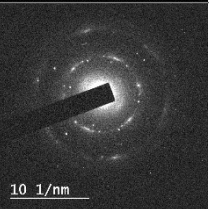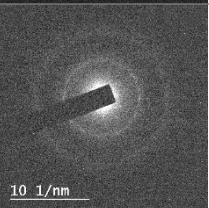| Source	Ratio GO/NiOHx	Ni (wt.%)	RSD (%)
Lactates	20	2.5	2.0
	10	4.1	3.4
	4	10.3	4.4
Nitrates	20	3.8	6.1
	10	6.9	0.3
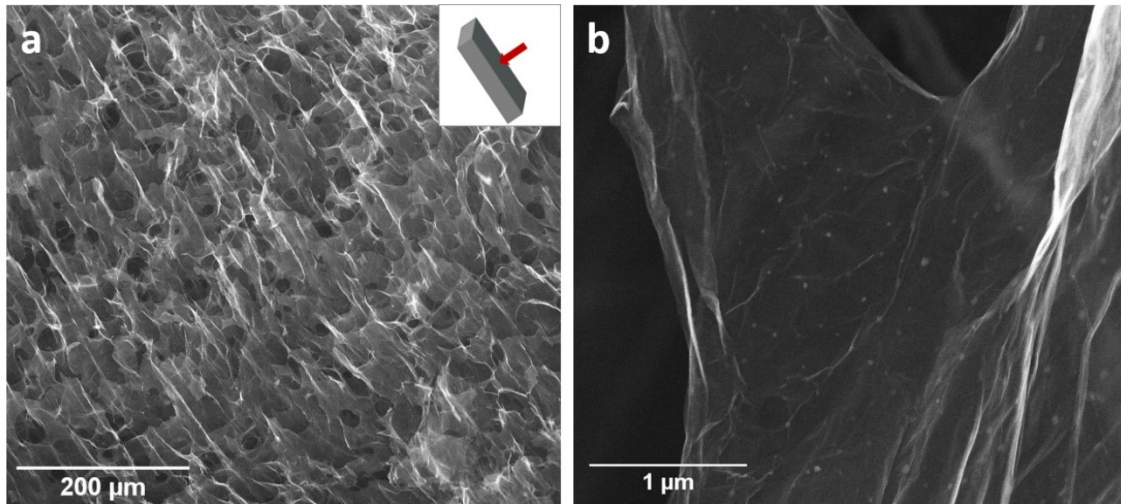
Figure *S3*|SEM images of rGO-6.9-Ni-nitrates. Image **a** was taken in a parallel plane to the direction of ice growth and **b** shows the dispersion of Ni-based particles on the graphene flake at higher magnification

Table *S2*| Selected area electron diffraction (SAED) ring patterns taken from the Ni-doped rGO samples. Diameter measurements of the rings were made using the software ImageJ.

Sample	Image	Reciprocal of diameter (1/nm)			Average (1/nm)	Interplanar spacing (Å)		
						Calculated	Theoretical [3]	
							Ni	NiO
rGO-2.5-Ni-lactates		9.714	9.640	9.694	9.683	2.07	2.0316	2.0845
		16.759	16.599	16.757	16.705	1.20	1.2057	1.2453
rGO-4.1-Ni-lactates		9.467	9.483	9.464	9.471	2.11		
		16.466	16.370	16.409	16.415	1.22		
rGO-3.8-Ni-nitrates		9.816	9.693	9.615	9.708	2.06		
		16.763	16.733	16.857	16.784	1.19		
rGO-6.9-Ni-nitrates		9.719	9.786	9.756	9.754	2.05		
		16.972	16.673	16.787	16.811	1.19		
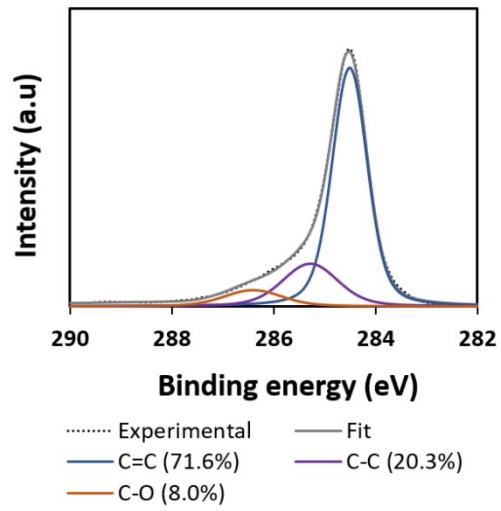
Figure *S4*. C1s spectrum of rGO at 650°C

Table *S3*|Ni/C surface ratio obtained by XPS analysis

Sample	Ratio Ni/C (%)
rGO-2.5-Ni-lactates	0.17
rGO-4.1-Ni-lactates	0.20
rGO-3.8-Ni-nitrates	0.32
rGO-6.9-Ni-nitrates	0.21

Table *S4*. Summary of results related to OER activity for our materials and similar composition materials reported in the literature.

| Material	Overpotential@ XmA/cm² (mV)	Electrode mass loading (mg/cm²)	Catalyst content wrt to carbon (%)	Tafel slope (mV dec⁻¹)	Electrolyte	Ref
Ni-based catalysts supported on graphene based materials						
Ni/NiO@rGO	480@10	ns	42	41	0.5M KOH	[4]
RGO-NiO/Ni-300C	>570	0.24	90	147	1 M KOH	[5]
RGO-NiO/Ni-500C	530@10	0.24	90	81	1 M KOH	[5]
RGO-Ni-Fe Foam -500C	480@10	0.24	48	57	1 M KOH	[6]
RGO-Ni-Fe-HT	390@10	0.24	70	75	1 M KOH	[6]
CoNi/GNR	430@10	0.15	40	131	1M KOH	[7]
GNiPy350N	320@10	0.15	30	136	1M KOH	[8]
Ni0.9Fe0.1/NC (20wt.%)	400@10	0.2	20	-	1M KOH	[9]
Ni0.9Fe0.1/NC (40wt.%)	350@10	0.2	40	-	1M KOH	[9]
Ni0.9Fe0.1/NC (60wt.%)	330@10	0.2	60	45	1M KOH	[9]
Ni0.9Fe0.1/NC (80wt.%)	300@10	0.2	80	-	1M KOH	[9]
Ni/NiO/GA$_{0.01}$	**1150**@**10**	**0.07**	**1.56**		**1M KOH**	[10]
Ni/NiO/GA$_{0.05}$	480@10	0.07	5.88		1M KOH	[10]
Ni/NiO/GA$_{0.1}$	410@10	0.07	12.0	69	1M KOH	[10]
Ni/NiO/GA$_{0.2}$	370@10	0.07	22.6	61	1M KOH	[10]
Ni/NiO/GA$_{0.4}$	320@10	0.07	40		1M KOH	[10]
rGO-2.5-Ni-lactates	**457**@**10**	**0.1**	**2.5**	**122.9**	**1M KOH**	
rGO-4.1-Ni-lactates	**432**@**10**	**0.1**	**4.1**	**95.3**	**1M KOH**	
rGO-10.3-Ni-lactates	**430**@**10**	**0.1**	**10.3**	**105.7**	**1M KOH**	**This work**
rGO-3.8-Ni-nitrates	**458**@**10**	**0.1**	**3.8**	**115.4**	**1M KOH**	
rGO-6.9-Ni-nitrates	**431**@**10**	**0.1**	**6.9**	**98.5**	**1M KOH**	
Influence of Fe on Nickel based catalysts						
RuO$_2$/NF	**317**@**100**	**0.2**	**100**	**106.4**	**1M KOH**	[11]
Ru-Ni(Fe)P$_2$/NF	**251**@**100**	**0.2**	**100**	**91.6**	**1M KOH**	[11]
Ru-NiP$_2$/NF	**253**@**100**	**0.2**	**100**	**125.1**	**1M KOH**	[11]
NiFe/Fe-MoO$_2$	**213**@**20**	**8.6**	**52**	**48**	**1M KOH**	[12]
Ni/MoO$_2$	**289**@**20**	**9.7**	**52**	**135**	**1M KOH**	[12]
MoO$_2$	**340**@**20**	**6.2**	**100**	**162**	**1M KOH**	[12]
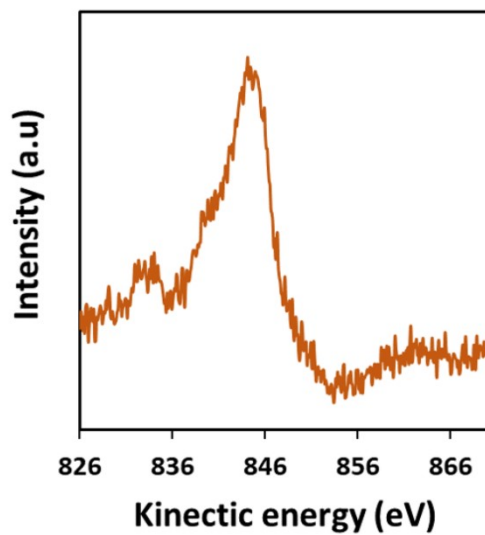
Figure *S5*. Ni LM[...]l by XPS analysis
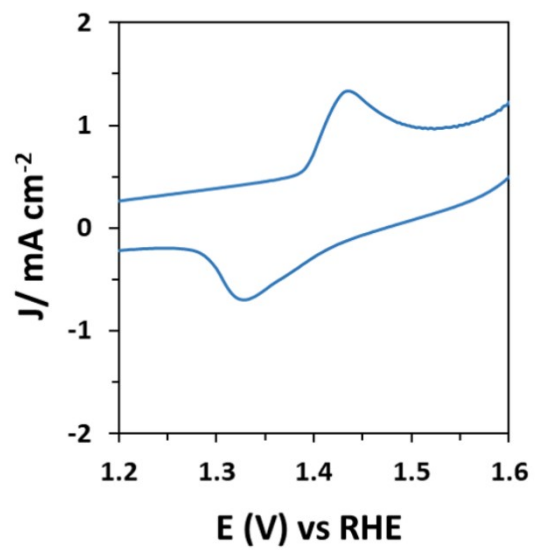
Figure *S6* | Redox peaks corresponding to the oxidation of Ni(OH)$_2$ to NiOOH (anodic peak) at 1.44V and the reverse reduction process (cathodic peak) at 1.33V
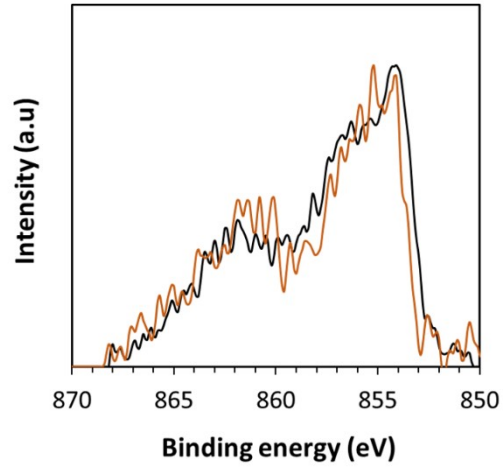
Figure *S7* | Ni 2p$_{3/2}$ XPS spectrum of rGO-4.1-Ni-lactate sample processed by freeze-casting (black) or tape-casting (orange)

Table *S5*| Values related to double-layer capacitance (C_{dl}) and electrochemical surface area (ECSA) obtained from all the samples prepared in this work. R_{ct} values obtained from impedance measurements are also shown.

Sample	Before OER stability test			After CP (10mAcm^{-2}, 12h)		
	C_{dl} (mF)	ECSA (cm²)	R_{ct} (Ω)	C_{dl} (mF)	ECSA (cm²)	R_{ct} (Ω)
rGO	0.38	9.50	262.40			
rGO-3.8-Ni-nitrates	0.59	14.75	46.10			
rGO-6.9-Ni-nitrates	1.57	39.25	19.67			
rGO-2.5-Ni-lactates	0.59	14.75	68.40			
rGO-4.1-Ni-lactates	0.50	12.50	18.07			
rGO-10.3-Ni-lactates	2.97	74.25	18.79	0.38	9.50	5.10

**Before OER stability test
(CP 12h @10mAcm⁻²)**

a

b

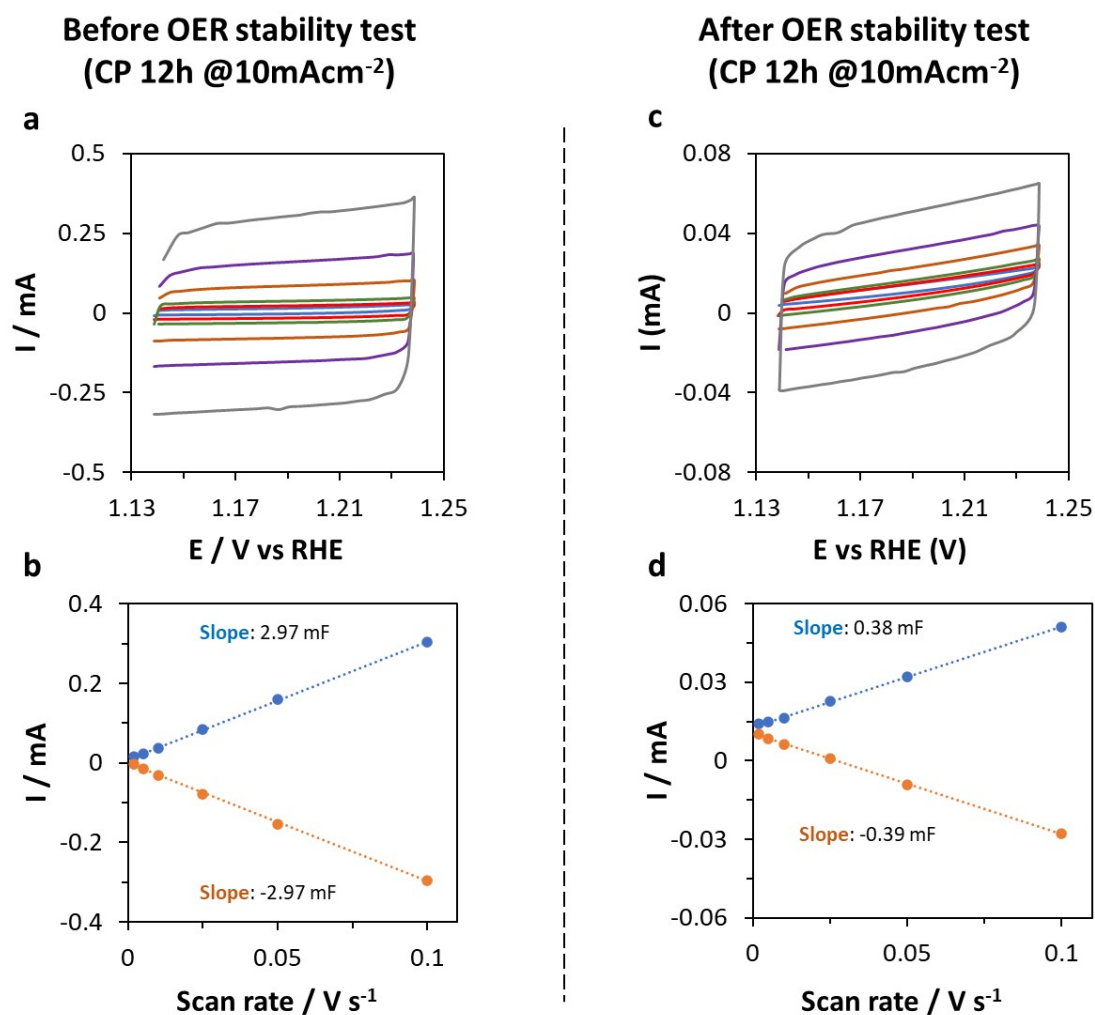**After OER stability test
(CP 12h @10mAcm⁻²)**

c

d

Figure *S8* | Double-layer capacitance measurements for determining electrochemically active surface area of rGO-10-Ni-lactates in 1 M KOH. (a,c) Cyclic voltammograms before and after OER stability test measured in a non-Faradaic region of the voltammogram at the following scan rate: (–) 0.002, (–) 0.005, (–) 0.010, (–) 0.025, (–) 0.05, (–) 0.1 Vs⁻¹. All current is assumed to be due to capacitive charging. (b) The cathodic (•) and anodic (•) charging currents measured at 1.2 V vs. RHE were plotted as a function of scan rate. The double-layer capacitance of the system (C_{dl}) is calculated as the average of the absolute slopes obtained from linear fits to the data. The electrochemically active surface area (ECSA) of the catalysts can be calculated by dividing C_{dl} by the specific capacitance of the sample (C_s: 0.040 mFcm⁻² in KOH 1M) as shown in the following equation:
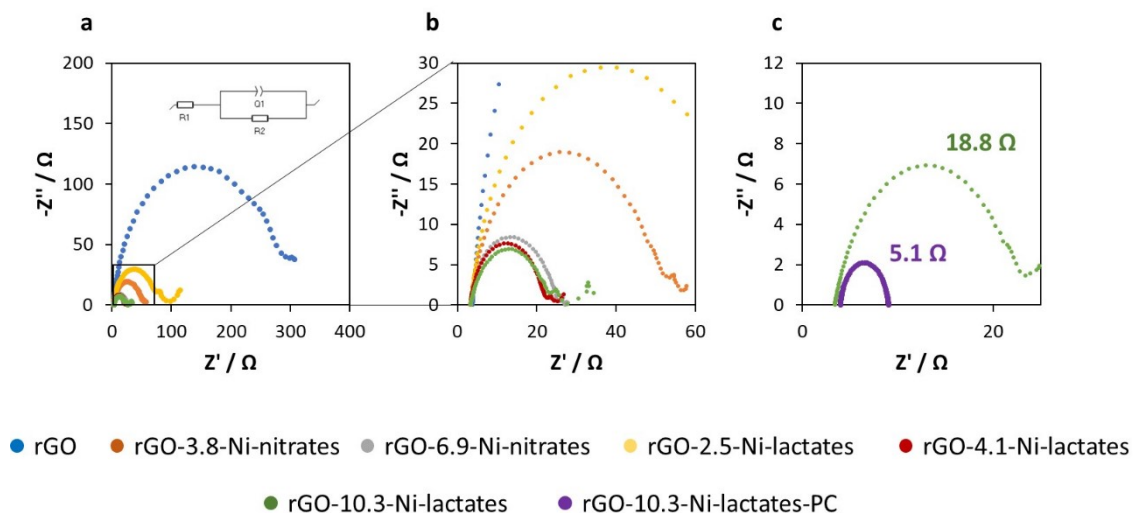
$$ECSA = \frac{C_{dl}}{C_s}$$

Figure *S9* | Nyquist plots of the different samples in N_2-saturated KOH 1M before OER stability test (a,b) and change in the EIS result for rGO-10.3-Ni-lactates after CP at 10 mAcm^{-2} for 12 hours (c). The conditions of the EIS experiment were 10 mV of potential perturbation with a frequency range between 100 kHz and 100 mHz. For EIS acquisition a constant potential of 1.7 V vs RHE was applied.
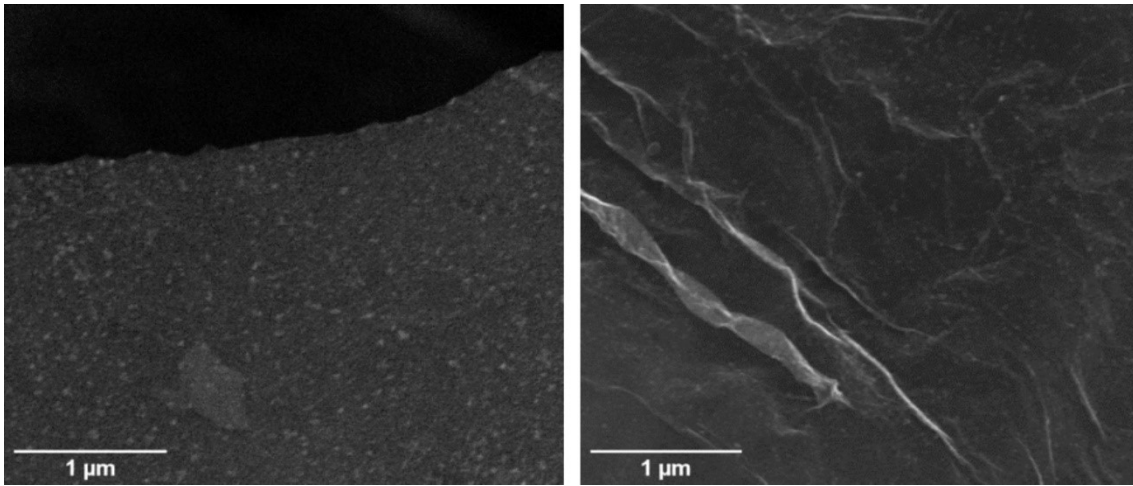
Figure *S10* | Scanning electron micrographs (SEM) of rGO-10.3-Ni-lactates aerogel taken using electro dispersive electrons.
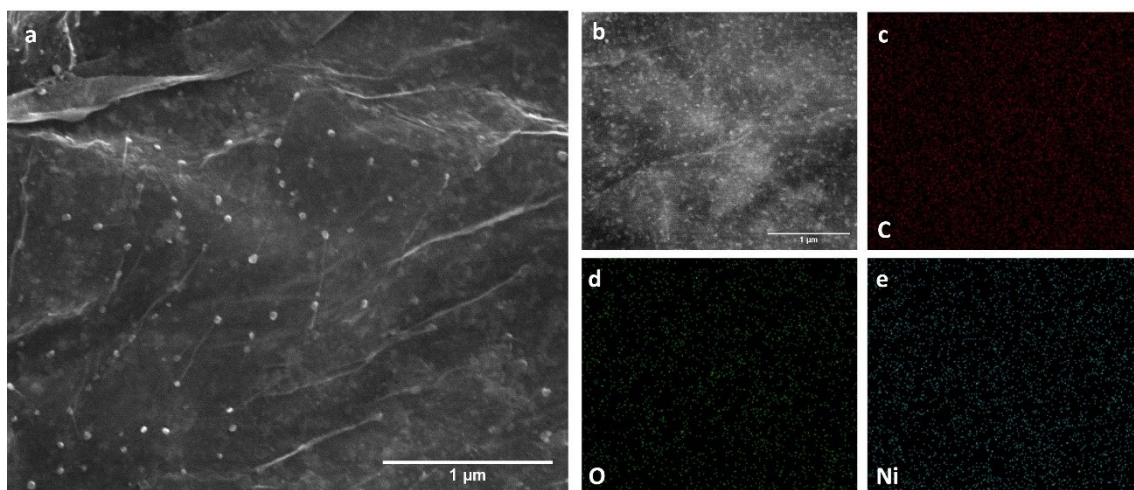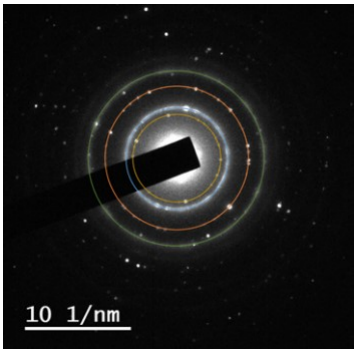
Figure *S11* | | SEM-EDS characterization. SEM images of rGO-10.3-Ni-lactates drop-casted into a graphite disc electrode taken using electro dispersive (a) and backscattered (b) electrons. EDS mapping elements on the same spot corresponding to carbon (c), oxygen (d) and nickel (e).

Table *S6*| Selected area electron diffraction (SAED) ring patterns taken from rGO-10.3-Ni-lactates. Diameter measurements of the rings were made using the software ImageJ.

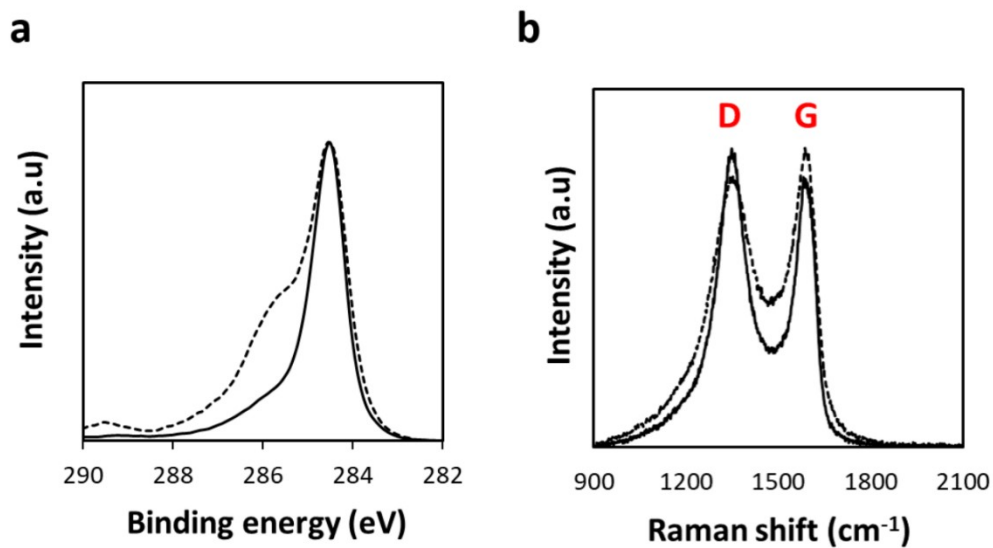| Reciprocal of diameter (1/nm)	Interplanar spacing (Å)	
	Calculated	Theoretical [3]NiO
8.356	**2.393**	**2.4094**
9.596	**2.084**	**2.0845**
13.556	**1.475**	**1.4763**
16.571	**1.207**	**1.2057**

Figure *S12* | Characterization of the carbon-based material. C1s spectra (**a**) and Raman profile (**b**) of rGO (solid line) and rGO-10.3-Ni-lactates (dashed line).
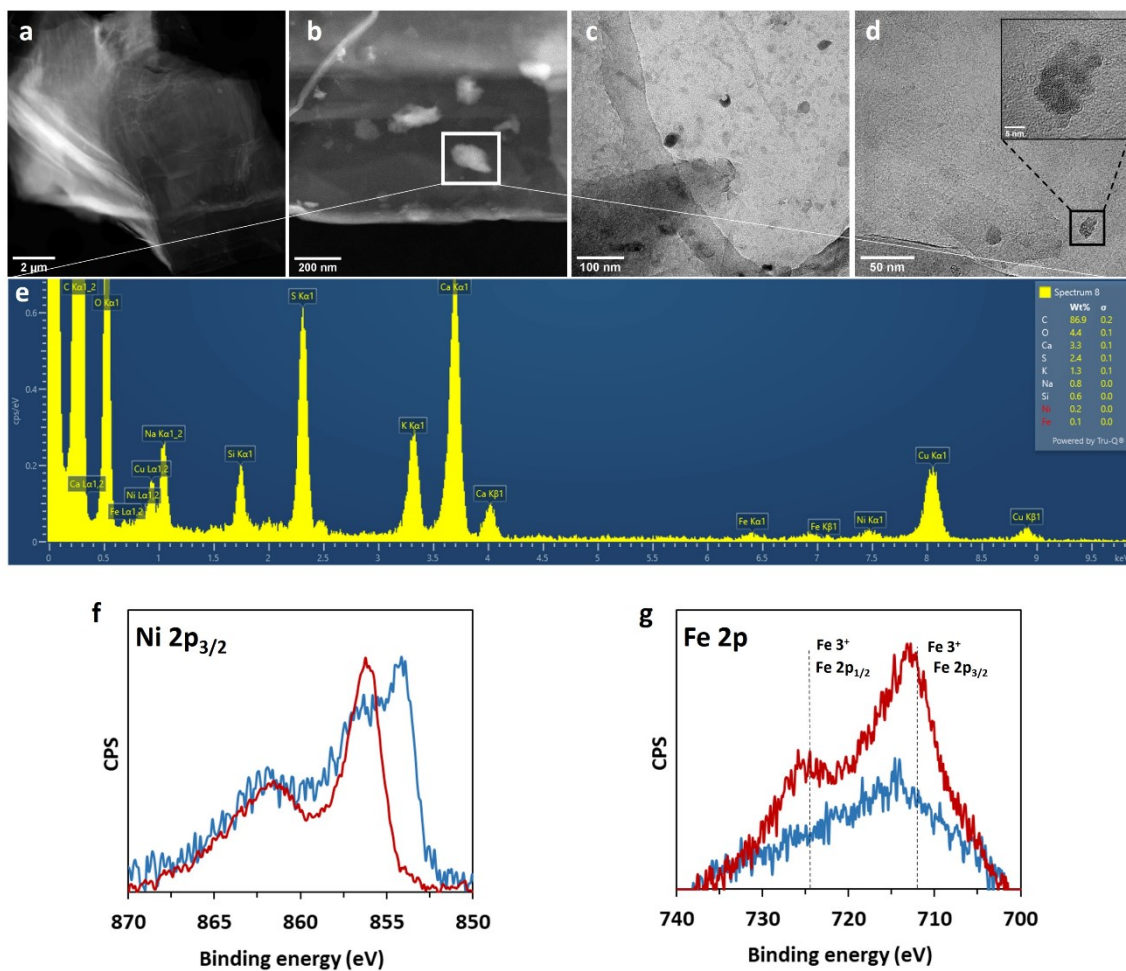
Figure *S13* | Post-catalysis characterization of rGO-4.1-Ni-lactates. STEM (a,b) and TEM (c,d) images of the sample. The inset in d corresponds with HR-TEM of a particle. EDX analysis was also carried out (e). Spectra of Ni 2p$_{3/2}$ (f) and Fe 2p (g) of the sample before (blue) and after the conditioning method (CP 10 mAcm^{-2} for 12 h) (red) were compared.

Table *S7*| Comparison of the influence of Fe impurities in different Ni-based materials reported in the literature. The comparison is made in terms of times-fold increase of the current density achieved after a conditioning method that involves the incorporation of Fe from impurities in the electrolyte.

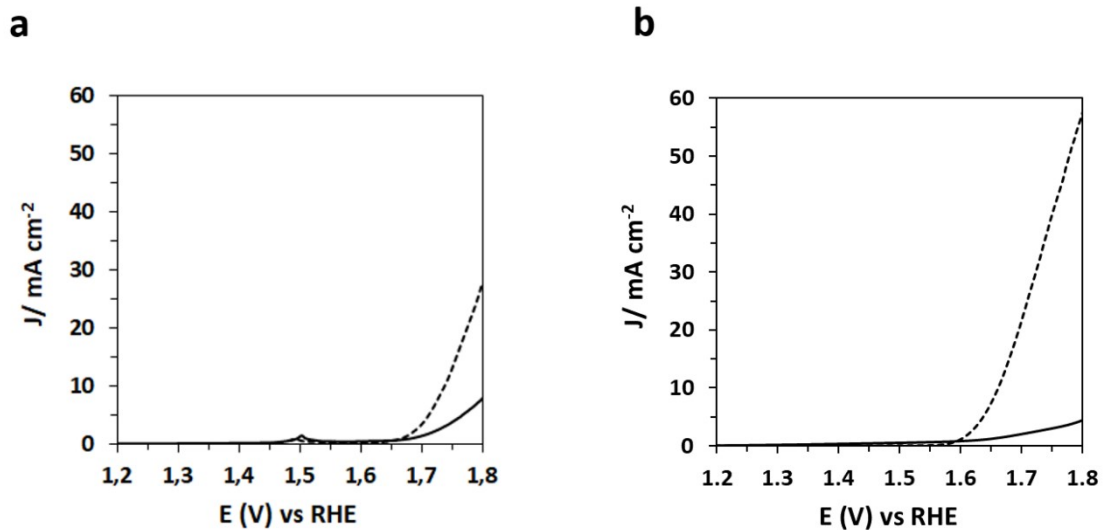| Sample	Conditioning method (CM)	Current density (J / mAcm-2)		Potential (V vs RHE)	Times-fold increase	Ref
		Before CM	After CM			
NiO_xH_y film	CA 1.5 V vs RHE 3 h	8.5	17.0	≈2.00	2.0	[13]
Ni film	1.0-1.8 V vs RHE 200 CV	2.4	8.4	1.53	3.5	[14]
Ni foil	CP 5 mAcm^{-2} 24 h	19	42.5	1.63	2.2	[15]
rGO-4.1-Ni-lactates	CP 10 mAcm^{-2} 12 h	5	58	1.80 V	11.6	This work

Figure *S14* | Improving in OER activity. LSV experiments at $1mVs^{-1}$ before (solid line) and after CP at $10mAcm^{-2}$ during 12h (dashed line) are shown for Ni(OH)2 drop-casted film (**a**) and rGO-4.1-Ni-lactates (**b**). Experiments were carried out in N_2-saturated 1M KOH.
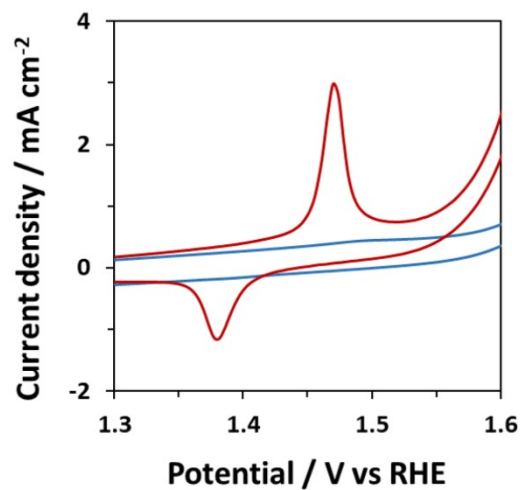
Figure *S15* | CV experiment of rGO after CP for 12 hours using KOH 1M (blue) and KOH 1M Fe-free (red)

References

1   L. Trotochaud, S. L. Young, J. K. Ranney and S. W. Boettcher, *J Am Chem Soc*, 2014, **136**, 6744–6753.

2   L. Liu, L. P. Twight, J. L. Fehrs, Y. Ou, D. Sun and S. W. Boettcher, *ChemElectroChem*, , DOI:10.1002/celc.202200279.

3   M. Niculescu and P. Budrugeac, Revue Roumaine de Chimie, 2013, vol. 58(4):381-386.

4   S. S. Narwade, S. M. Mali, R. V. Digraskar, V. S. Sapner and B. R. Sathe, *Int J Hydrogen Energy*, 2019, **44**, 27001–27009.

5   D. Wang, F. Watanabe and W. Zhao, *ECS Journal of Solid State Science and Technology*, 2017, **6**, M3049–M3054.

6   D. Wang, F. Watanabe and W. Zhao, *J Electrochem Soc*, 2016, **163**, F3158–F3163.

7   L. S. Bezerra and G. Maia, *J Mater Chem A Mater*, 2020, **8**, 17691–17705.

8   A. S. Souza, L. S. Bezerra, E. S. F. Cardoso, G. V. Fortunato and G. Maia, *J Mater Chem A Mater*, 2021, **9**, 11255–11267.

9   X. Zhang, H. Xu, X. Li, Y. Li, T. Yang and Y. Liang, *ACS Catal*, 2016, **6**, 580–588.

10   F. E. Sarac Oztuna, T. Beyazay and U. Unal, *Journal of Physical Chemistry C*, 2019, **123**, 28131–28141.

11   D. Wu, B. Liu, R. Li, D. Chen, W. Zeng, H. Zhao, Y. Yao, R. Qin, J. Yu, L. Chen, J. Zhang, B. Li and S. Mu, Small, 2023, 19, 2300030

12   W. Shi, J. Zhu, L. Gong, D. Feng, Q. Ma, J. Yu, H. Tang, Y. Zhao and S. Mu, *Small*

13   R. Farhat, J. Dhainy and L. I. Halaoui, *ACS Catal*, 2020, **10**, 20–35.

14   F. Bao, E. Kemppainen, I. Dorbandt, F. Xi, R. Bors, N. Maticiuc, R. Wenisch, R. Bagacki, C. Schary, U. Michalczik, P. Bogdanoff, I. Lauermann, R. Van De Krol, R. Schlatmann and S. Calnan, *ACS Catal*, 2021, **11**, 10537–10552.

15   Y. J. Son, S. Kim, V. Leung, K. Kawashima, J. Noh, K. Kim, R. A. Marquez, O. A. Carrasco-Jaim, L. A. Smith, H. Celio, D. J. Milliron, B. A. Korgel and C. B. Mullins, *ACS Catal*, 2022, **12**, 10384–10399.